JOURNAL OF PROPULSION AND POWER
Vol. 17, No. 6, November–December 2001

# Investigation of Kerosene Combustion Characteristics with Pilot Hydrogen in Model Supersonic Combustors

G. Yu,* J. G. Li,† X. Y. Chang,‡ and L. H. Chen§
*Chinese Academy of Sciences, 100080 Beijing, People's Republic of China*
and
C. J. Sung¶
*Case Western Reserve University, Cleveland, Ohio 44106*

**Experimental investigations on the ignition and combustion stabilization of kerosene with pilot hydrogen in Mach 2.5 airflows were conducted using two test combustors, with cross sections of 30.5 × 30 and 51 × 70 mm, respectively. Various integrated modules, including the combinations of different pilot injection schemes and recessed cavity flameholders with different geometries, were designed and tested. The stagnation pressure of vitiated air varied within the range of 1.1–1.8 MPa, while the stagnation temperature varied from 1500 to 1900 K. Specifically, effects of the pilot hydrogen injection scheme, cavity geometry, and combustor scaling on the minimally required pilot hydrogen equivalence ratio were systematically examined. Results indicated that the cavity depth and length had significant effects on the ignition and flameholding, whereas the slanted angle of the aft wall was relatively less important. Two cavities in tandem were shown to be a more effective flameholding mechanism than that with a single cavity. The minimally required pilot hydrogen equivalence ratio for kerosene ignition and stable combustion was found to be as low as 0.02. Furthermore, combustion efficiency of 80% was demonstrated to be achievable for kerosene with the simultaneous use of pilot hydrogen and a recessed cavity to promote the ignition and global burning.**

## Introduction

LIQUID hydrocarbons are attractive candidates for fueling scramjet engines in Mach number $\leq 8$ flight regimes due to their significant benefits in terms of energy density and handling issues, as compared to hydrogen. However, there are also shortcomings regarding the use of hydrocarbon fuels in supersonic combustion. Notably, their relatively long ignition delay times typically exceed the residence time of gas flow within combustors.[1,2] Moreover, liquid hydrocarbons require quick vaporization before mixing and the subsequent combustion.

Research devoted to the improvement of hydrocarbon combustion in supersonic flow has been in progress. Many studies[3–7] have demonstrated that a hydrogen pilot flame can provide high-temperature reacting gas with a large radical pool so that the subsequent hydrocarbon ignition is enhanced. Investigations of supersonic combustion of both gaseous and liquid hydrocarbon fuels with hydrogen addition, such as methane,[8] ethylene,[9] toluene,[3] kerosene,[10] and endothermic fuels,[1,11,12] have been reported. Among them, the endothermic fuels have drawn considerable attention due to their unique advantages in simultaneously meeting the requirements of combustion intensity and engine cooling. In practice, the endothermic fuel is first heated and catalytically cracked or dehydrogenated at the point of flash vaporization, which is subsequently used as a coolant before reaching the combustor.

Whereas the utilization of the endothermic fuels and their integration into practical systems merit further studies, liquid hydrocarbons, such as kerosene, with hydrogen addition can be treated as an alternative. Investigations of the supersonic combustion characteristics of this dual kerosene–hydrogen system can also provide insights into the supersonic combustion of other aeropropulsion fuels. Practical issues of particular interest include the extent of the combustion enhancement due to pilot hydrogen, the amount of pilot hydrogen required, and the associated combustion performance.

In recent years, the use of wall cavities as a flameholder in supersonic combustors has attracted extensive attention.[13–15] With a cavity, a high-temperature, low-speed recirculation, reaction zone can be established to serve as a pilot flame, which can in turn reduce the bulk ignition delay time and sustain a stable combustion. Cavity flameholders, such as rear-facing step and recessed cavity, were investigated theoretically and experimentally.[3,6,16–18] In particular, Bonghi et al.[3] used a rearward-facing step as the main flameholding mechanism to study a toluene-fueled combustor, in which toluene was injected normal to a Mach 2.5 flow at a stagnation temperature of 1000 K. The investigations found[3] that the pilot hydrogen flame was limited to an equivalence ratio of 0.05, in which stable combustion of toluene at an equivalence ratio of 0.13 was sustained. Moreover, for a Mach 6 flight, Vinogradov et al.[6] used plate and cavity flameholders and employed various combinations of strut and wall injection with both pilot hydrogen and liquid kerosene to obtain stable combustion at kerosene equivalence ratios as high as 0.6 and pilot hydrogen equivalence ratio as low as 0.1. Owens and Segal[16] reported that the pilot hydrogen equivalence ratio could be reduced to be as low as 0.02 by using a rear-facing step, and the associated kerosene combustion efficiency was about 60%, for a Mach 4.75 flight in a combustor with cross section of 25.4 × 25.4 mm. Furthermore, Yu et al.[14] pointed out that an integrated fuel injector–flameholder using a simple cavity would be a viable approach to enhance scramjet performance.

Recognizing that liquid hydrocarbons are the preferred aeropropulsion fuels in many applications and that a cavity flameholder holds great potential to achieve active flame stabilization in high-speed flows, the present study aimed to investigate experimentally the combustion characteristics of kerosene-fueled model supersonic combustors coupled with pilot hydrogen injection. Experiments were conducted using combustors with a fixed entry Mach number of 2.5, at various stagnation conditions and global equivalence

Received 2 January 2001; revision received 30 May 2001; accepted for publication 3 June 2001. 

*Professor, Institute of Mechanics, 15 Zhongguancun Road, Haidian District; yugong@mail.imech.ac.cn. Member AIAA.
†Professor, Institute of Mechanics; jgli@mail.imech.ac.cn. Member AIAA.
‡Professor, Institute of Mechanics; changxy@mail.imech.ac.cn. Member AIAA.
§Associate Professor, Institute of Mechanics; lhchen@mail.imech.ac.cn.
¶Nord Assistant Professor, Department of Mechanical and Aerospace Engineering, 10900 Euclid Avenue; cjs15@po.cwru.edu. Senior Member AIAA.

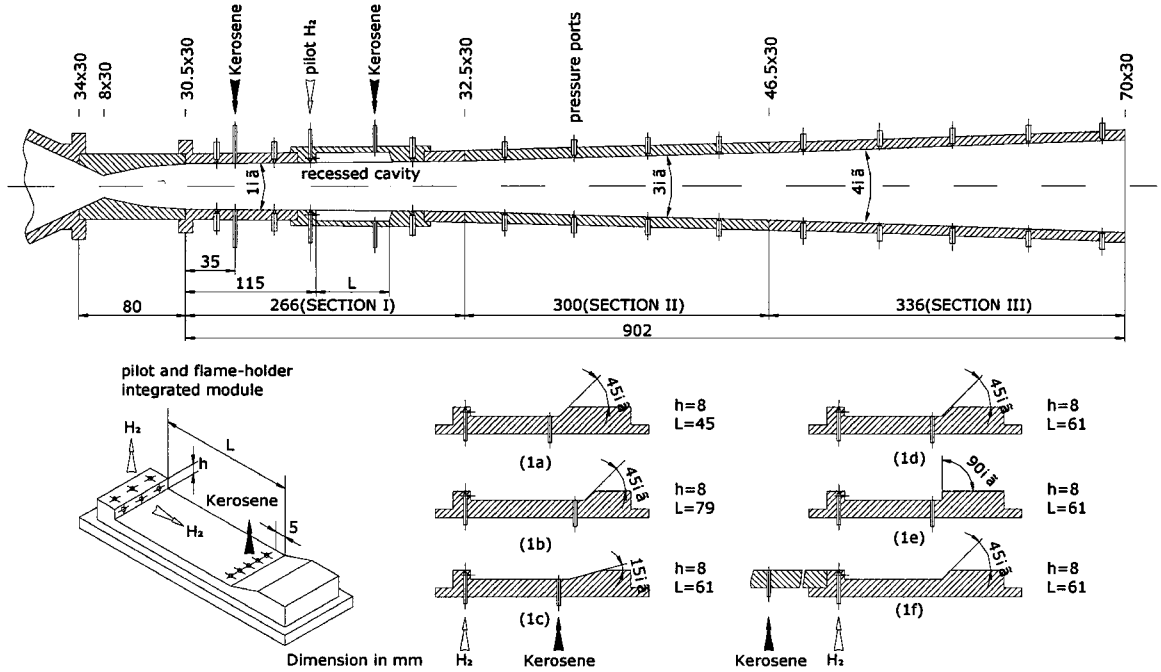


**Fig. 1 Schematic of kerosene/hydrogen supersonic combustor 1, all length dimensions in millimeters.**

ratios. Two combustors with different configurations were designed and tested. Combustor 1 had a cross section of 30.5 × 30 mm with a length of 902 mm, lengthened from a previous model combustor.[19] Combustor 2 had a cross section of 51 × 70 mm with a length of 1095 mm, which was designed to examine combustor scaling effects. The stagnation temperatures of vitiated air varied from 1500 to 1900 K and stagnation pressures ranged from 1.1 to 1.8 MPa. It is also noted that the combustor entrance condition of Mach 2.5 basically simulates Mach 6–7 flight.

The specific objectives of the present study are as follows. The first was to investigate experimentally the characteristics of self-ignition and flame stabilization for kerosene–hydrogen dual-fuel system in model supersonic combustors. In addition, scaling effects on combustor performance were of particular interest. Hydrogen, serving as a pilot flame, was injected into the airstream either downstream or upstream of the kerosene injection station. The chemical reaction of kerosene is expected to be locally accelerated by the faster hydrogen reaction and to be further promoted by the low-speed recirculation flow, as well as the local high-temperature gas inside the recessed cavity. Thus, the bulk flame is expected to be anchored by the flame segment in the local region of slow flow velocity and high chemical reactivity. Integrated modules of pilot hydrogen injection and cavity flameholder with different geometries were designed and tested. The atomization, penetration, and spreading of a kerosene jet spray in a Mach 2.5 flow were also visualized. Furthermore, based on the measured static pressure distribution inside the combustor, a one-dimensional analysis developed previously[20,21] was used for the data reduction and assessment of the combustor performance.

The experimental details of the investigation are presented in the next section, which is subsequently followed by results and discussion.

## Experimental Considerations

### Facility and Experimental Specifications

*Vitiated Air Supply System*

High-temperature vitiated air was provided by burning hydrogen, oxygen, and air in a heater with the resulting oxygen volume fraction equal to that of the normal air. The system was controlled by a computer and capable of supplying heated air up to flow rate of 1.5 kg/s, stagnation temperature of 2100 K, and stagnation pressure of 4.5 MPa. The airflow was then accelerated to Mach 2.5 with a two-dimensional nozzle. All of the flow rates were metered by sonic nozzles. The uncertainty associated with the flow rate measurement was estimated to be within 3%. The stagnation temperature $T_t$ was measured by B-type thermocouples with corrections of radiation, conduction, and thermal inertia, which was further compared with the computed value based on the measured stagnation pressure and reactant flow rates. The experimental error in the stagnation temperature measurement was within 3% for $T_t < 2000$ K. Details of this facility were described by Li et al.[22]

*Combustor Configurations*

Figure 1 shows the schematic of combustor 1 that had an entrance cross section of 30.5 × 30 mm. It was composed of three sections, including a nearly constant area section (1-deg divergence for boundary-layer corrections) of 266 mm length (section I) and two expansion sections (sections II and III). The first expansion section (section II) was of 300 mm length and had 3-deg divergence, whereas the second expansion section (section III) was 336 mm long with 4-deg divergence.

The systems of pilot injectors and recessed flameholder cavities were designed to be composed of interchangeable, integrated modules for flexible variations of system configuration. According to the results of Li et al.,[19] the cavity depth $h$ of combustor 1 was selected as $h = 8$ mm. Additionally, the lengths of the cavity bottom floor, $L$, were $L = 45$, 61, and 77 mm, whereas the slanted angles were 15, 45, and 90 deg. The different combinations denoted as a–f are shown in Fig. 1. Pilot injection was also designed to be flexible via orifices of 1.2 mm diameter, including: 1) parallel injection to the main flow from the base of the front cavity wall, 2) normal injection to the main flow, and 3) simultaneous injections in the directions parallel and normal to the main flow. Kerosene was injected via a 0.4- or 0.5-mm-diam orifice normal to the mainstream. The location of kerosene injection was mostly near the trailing edge of the cavity, namely, located at $5h$, $7h$, and $9h$ from the location of the pilot hydrogen injection station for modules 1a, 1c–1e, and 1b, respectively. For module 1f, however, kerosene was injected upstream of the cavity.

Figure 2 shows the schematic of combustor 2, which had an entrance cross section of 51 × 70 mm. This combustor was also composed of three sections. These included the nearly constant area 275-mm section with 1-deg divergence (section I), the expansion 420-mm section with 3-deg divergence (section II), and additional

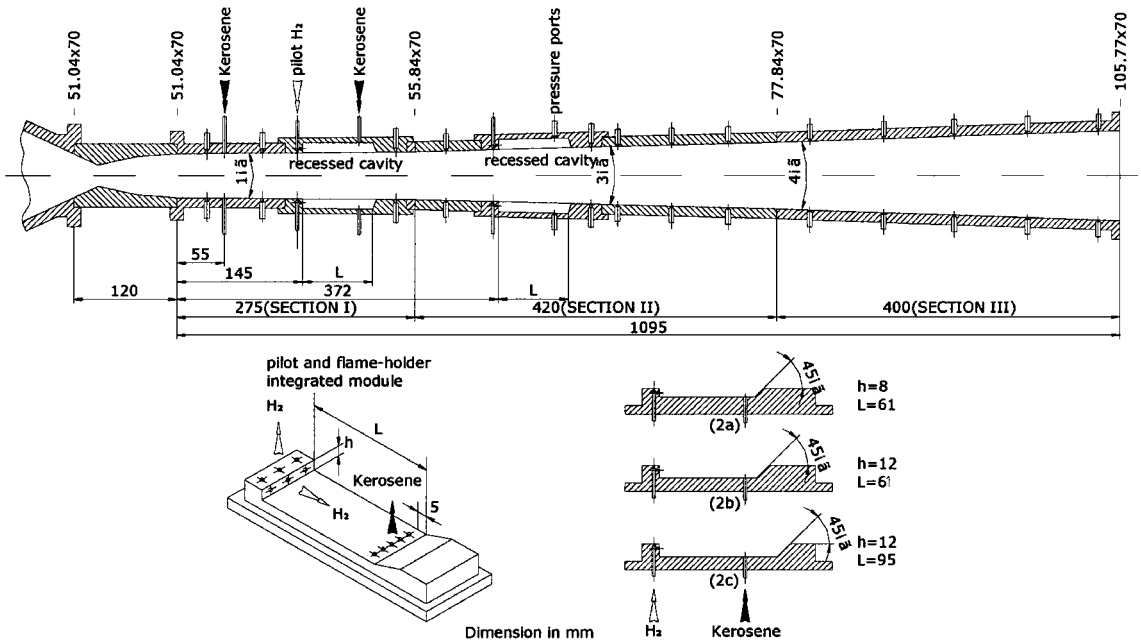


**Fig. 2 Schematic of kerosene/hydrogen supersonic combustor 2. Single cavity station was used in most cases. For the case of two cavities in tandem, one cavity module was installed in section I and the other identical one was install in section II, all length dimensions are in millimeters.**

expansion section 400 mm long with 4-deg divergence (section III). Integrated pilot and flameholder modules were $h = 8$ mm and $L = 61$ mm (module 2a), $h = 12$ mm and $L = 61$ mm (module 2b), and $h = 12$ mm and $L = 95$ mm (module 2c) all of the aft ramp angles were fixed as 45 deg. Pilot hydrogen was injected in both parallel and normal directions via three orifices of 1.2 mm diam. Kerosene was injected normal to the mainstream via five orifices of 0.45 mm diam located at the trailing edge of the cavity, as shown in Fig. 2.

*Pressure Measurements*

Static pressures were measured along the axial direction of the flow path. There were 24 pressure ports arranged along each of the two neighboring sidewalls of the model combustor. To obtain a mean axial pressure distribution, pressure data of two sidewalls measured at the same axial location were averaged. Motorola MPX2200 0–0.5 MPa pressure sensors were used to detect the static pressure signal. The uncertainty associated with the static pressure measurement was estimated to be within 2%.

Moreover, the total pressure at the exit of the model combustor was measured by using the water-cooled pitot probes. The pressure sensor employed was Sensym 19CIU300 0–1.5 MPa. The experimental error in the total pressure measurement was within 3%.

*Kerosene Atomization*

Kerosene spray was achieved by pressurizing the liquid fuel in the cylinder through a piston. The kerosene flow rate was measured by the actual amount of kerosene released from the kerosene cylinder divided by time elapsed.

Note that the performance of the liquid hydrocarbon-fueled combustor strongly depends on the rapid vaporization and the uniform distribution of the droplets in a fuel spray. Moreover, the droplet vaporization rate mainly depends on the type of fuel, the freestream temperature, the ambient composition, and the size of the droplet. When the analysis of Kanury[23] is followed, the variations of kerosene evaporation time with the droplet diameter were estimated at the temperature range from 1000 to 1500 K. The results indicated that in this temperature range the droplet evaporation time rapidly decreases with decreasing droplet size and could be limited to within 1 ms as long as the droplet diameter is smaller than 20 $\mu$m. When it is recognized that the typical cavity residence time is about few milliseconds, it is, therefore, preferable to control the droplet diameter size to be around 20 $\mu$m or less.

**Kerosene Droplet Size and Spray Visualization**

The average droplet diameters of the kerosene sprays with different injector diameters were measured using a Malvern 2600/3600 particle sizer. Results showed that with injector diameter of 0.4 mm, the mean droplet diameter decreased from 25.2 to 20.2 $\mu$m as the injection pressure was increased from 2.1 to 4.5 MPa. The measured mean droplet diameter of the spray was found to be about the same with injector orifice diameters of 0.4 and 0.5 mm. It was further shown that the dependence of droplet size on the injecting pressure was quite insignificant in the injecting pressure range of 2.1–4.5 MPa.

Spray visualization was accomplished through the view windows installed on both sides of the kerosene injection station. The view windows consisted of a pair of quartz plates, 66 mm in height and 120 mm in length. Figure 3 shows the direct photographs taken in combustor 2 without the installation of any cavity module, illustrating the penetration and spreading of the kerosene jet spray. Kerosene was injected normal to the main flow at the same location as those shown in Fig. 2. Moreover, Figs. 3a–3c corresponded to the cases with injection pressure of 4.5, 3.5, and 2.5 MPa, respectively. The airflow was Mach 2.5, while the local pressure was 0.08 MPa, and the local temperature was 800 K.

Figure 3 demonstrates several features of the atomization process. First, there was a small atomization region ahead of the main spray, suggesting that the spray also spread toward the upstream direction from the injection location. As a result, a detached bow shock wave was expected to exist just upstream of the spray jet. This bow shock would lead to the upstream wall boundary-layer separation and a low-speed recirculating zone. In addition, due to the compressive nature of the bow shock wave, the kerosene droplet concentration appeared to be much higher in the region close to the interface separating the main spray and the freestream. Such a heterogeneous distribution of the atomization was seen to improve substantially along the downstream direction. Furthermore, it was found experimentally that the extent of penetration and the spreading rate of atomization increased about 30% by increasing injection pressure from 2.5 to 4.5 MPa.

**Ignition Delay Times**

Because the detailed kinetics mechanism of kerosene is not currently available, the estimation of its ignition delay time has to

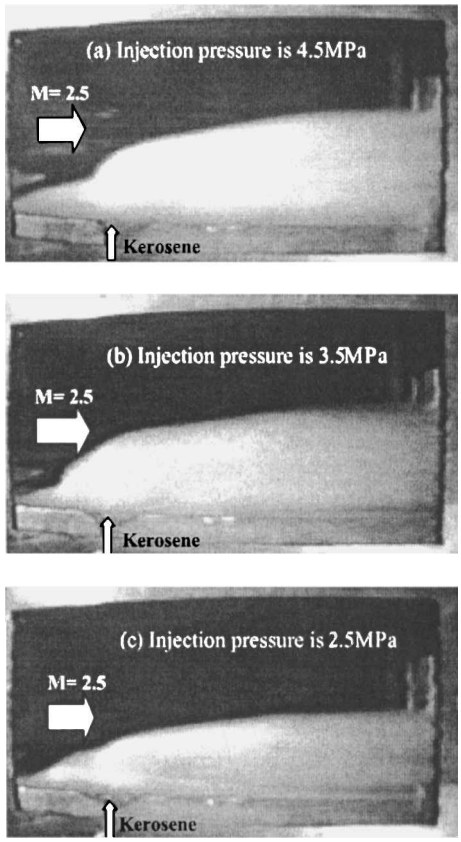


**Fig. 3 Penetration and spreading of kerosene jet spray in a Mach 2.5 flow, with various injection pressures: a) injection pressure = 4.5 MPa, b) injection pressure = 3.5 MPa, and c) injection pressure = 2.5 MPa.**

use the empirical correlation. Veretennicov[24] compiled and compared most of the previous reported data. It was concluded[24] that an empirical dependence of ignition delay times for kerosene was in good agreement with Mullins's data,[25] which was expressed as $10^{-10} \times e^{(Ea/RT)}/p$ (seconds), where $E_a = 41$ kcal/mole is the overall activation energy, $R$ the universal gas constant, $T$ the temperature (degrees Kelvin), and $p$ the pressure (atmosphere, standard). As such, although the atmospheric ignition delay time given by the preceding correlation can be as high as 90 ms at the temperature of 1000 K, it decreases rapidly with increasing temperature. For example, the ignition delay of kerosene is reduced below 1 ms when $T > 1280$ K. Again, if the cavity residence time is of few milliseconds the local high temperature within the cavity flameholder has to be greater than 1280 K so that the self-ignition of kerosene is possible.

#### Experiment Procedure

The typical tests lasted 7 s using a preprogrammed sequencer. In the heater, the major gases (air, oxygen, and hydrogen) were released 1 s after a spark ignited the pilot mixture of air and hydrogen. It generally took ~1.5 s to reach a steady state and to achieve the required temperature and pressure. Once the steady Mach 2.5 airflow was established (at 2.475 s), the pilot hydrogen was injected and subsequently self-ignited if the condition was adequate. It took another 2 s to achieve a steady burning for the given pilot hydrogen and airflow. Kerosene was then injected at 4.5 s. Once the pilot hydrogen flame ignited the kerosene, the overall kerosene burning would be sustained even after the pilot hydrogen ceased. Note that although the combustor walls were not specially cooled, at various conditions the measured wall temperature ranged between 327 and 395 K even when stable kerosene combustion was established.

## Data Reduction

When the studies of Yu et al.,[20,21] were followed, a one-dimensional model was developed to facilitate the data reduction and the subsequent performance assessment, in a two-stage manner. The details of the one-dimensional model have been documented in Refs. 20 and 21. First, the flowfield within the combustor was approximated based on the measured distribution of static pressure. This approximated flowfield was then used as an input for the computation of the axial profiles of Mach number, static pressure, total pressure, static temperature, total temperature, and core flow area. Note that the computed core area of the flow is not necessarily equal to the actual cross-sectional area of the combustor.

Furthermore, the combustion efficiency is generally defined by the ratio of the static temperature increment between the exit and entrance of combustor to the temperature difference between the corresponding adiabatic flame temperature and the static temperature at the combustor entrance. When it is recognized that kerosene is a complex mixture, a simplified one-formula surrogate fuel model,[26] with $C_{12}H_{24}$ representing kerosene, was adopted. The associated thermodynamic properties taken from Wang,[26] including heat capacity, enthalpy, and entropy as a function of temperature, were used to calculate the adiabatic flame temperature.

Equivalence ratios of pilot hydrogen and kerosene in the mixture were calculated based on the assumption that hydrogen is first consumed completely with the available oxygen because of its small addition. Thus, the equivalence ratio of pilot hydrogen, $\phi_H$, is expressed by

$$\phi_H = (m_H/m_A)/(m_H/m_A)_{st}$$

where $m_H$ and $m_A$ are the mole flow rates of pilot hydrogen and vitiated air, respectively. The subscript st represents the stoichiometric condition, and hence, $(m_H/m_A)_{st} = 0.418$. Note that in the present heater setup the composition of the vitiated air depends on the resulting air temperature,[27] especially the level of water contamination. Whereas the mean molecular weight of the vitiated air varies with the specific stagnation temperature, the oxygen mole fraction within the resulting vitiated air is the same as that of normal air (20.9%). Therefore, the use of mole flow rate expedites the evaluation of fuel equivalence ratio.

Moreover, when the concept of Yu et al.[28] is followed, the effective equivalence ratio of kerosene is expressed by

$$\phi_F = m_F/[m_A - m_H/(m_H/m_A)_{st}]/(m_F/m_A)_{st}$$

where $m_F$ is the mole flow rate of kerosene and $(m_F/m_A)_{st} = 0.0116$ by approximating kerosene as $C_{12}H_{24}$. Additionally, this expression of the effective equivalence ratio assumes that to oxidize completely $m_H$ amount of pilot hydrogen, it requires $m_H/(m_H/m_A)_{st}$ amount of air and, hence, the remaining air, $[m_A - m_H/(m_H/m_A)_{st}]$, can then be used to oxidize $m_F$ amount of kerosene.

## Results and Discussion

#### Typical Static Pressure Distribution

Figure 4 shows the typical static pressure distribution at the relevant moments. Clearly, the axial pressure distributions along the

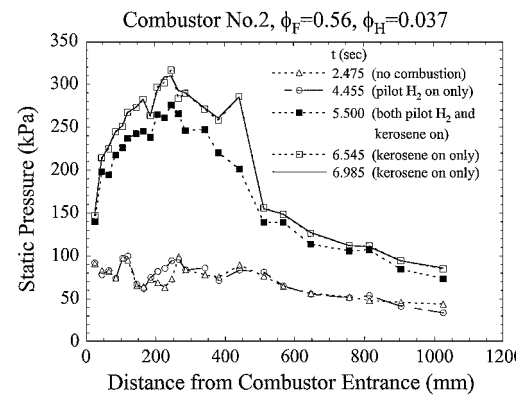


**Fig. 4 Typical static pressure distributions in the axial direction at relevant moments; uncertainty associated with the static pressure measurement was within 2%.**

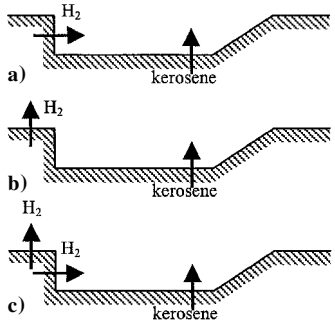


**Fig. 5 Three different pilot hydrogen injection schemes employed: a) parallel, b) normal, and c) simultaneously parallel and normal.**

combustor at different moments, namely, before the pilot hydrogen ignition (no combustion), after the pilot hydrogen burning, and after the kerosene burning, are seen to be different. In this run the pressure rise after the pilot hydrogen injection was less pronounced due to the relatively small amount of pilot hydrogen ($\phi_H = 0.037$). However, with the substantial amount of heat release by the subsequent kerosene combustion, the static pressure increased rapidly even starting at the upstream of kerosene injection station. Moreover, after the steady combustion of kerosene was sustained, the static pressure was seen to reach an approximately isobaric plateau within the section of nearly constant area (section I). Subsequently, the static pressure decreased continuously till the combustor exit because of the significant expansion process in the downstream divergent sections, as shown in Fig. 4. Furthermore, the pressure profile that extended toward the upstream of kerosene injection was consistent with the atomization visualization of kerosene jet spray shown in Fig. 3. Also note that the pilot hydrogen injection ceased at 5.5 s, whereas kerosene continued burning for additional 1.5 s till the end of experiment (at 7 s).

### Influence of Pilot Injection Scheme on Minimally Required Pilot Hydrogen Equivalence Ratio

A series of experiments was conducted in combustor 1 using cavity flameholder 1d (Fig. 1) to compare the effectiveness of three different pilot injection schemes. The three injection schemes included parallel (Fig. 5a), normal (Fig. 5b), and simultaneously parallel–normal injections, (Fig. 5c). Additionally, the flow conditions were kept approximately identical, namely, the stagnation temperature of 1750 K, stagnation pressure of 1.8 MPa, and the kerosene equivalence ratio of 0.2, despite different pilot injection schemes. Experimental results showed that the minimally required pilot hydrogen equivalence ratios, $\phi_{H,min}$, to sustain a stable kerosene combustion were 0.065, 0.04, and 0.025 for injection schemes shown in Figs. 5a–5c, respectively. Note that, although the value of $\phi_{H,min}$ might be test facility dependent, this remarkable difference yielded using the same model combustor is of significance. At least, the parallel pilot injection (Fig. 5a) did not seem to be the most effective scheme to promote the ignition and flameholding of kerosene as compared to the normal and the combined parallel–normal injection schemes. The differences in $\phi_{H,min}$ might be attributed to the distribution of pilot hydrogen within the cavity and its subsequent interaction with the kerosene injection. However, the detail reason is still not clear due to the strong interactions among the pilot hydrogen flame, the recirculation flow inside the recessed cavity, and kerosene injection. In particular, the interactions were also complicated by the presence of the oblique shock train and expansion waves within the cavity.

### Influence of Recessed Cavity Geometry on $\phi_{H,min}$

Figures 6–10 show the profiles of the static pressure along the axial direction yielded in combustor 1 using the integrated pilot-flameholder modules 1a–1e (cf., Fig. 1), respectively. Especially, three static pressure profiles at the relevant moments, which were before the pilot hydrogen injection ($t = 2.475$ s), after the pilot hydrogen injection ($t = 4.455$ s), and after the kerosene injection ($t = 6.490$ s), were selected and compared. The experimental flow

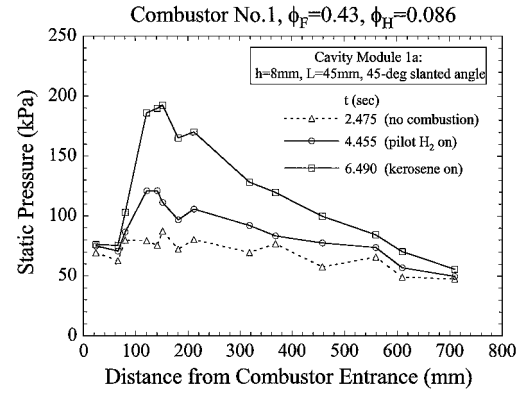


**Fig. 6 Static pressure distributions at relevant moments, using combustor 1 with the integrated cavity module 1a, shown in Fig. 1.**

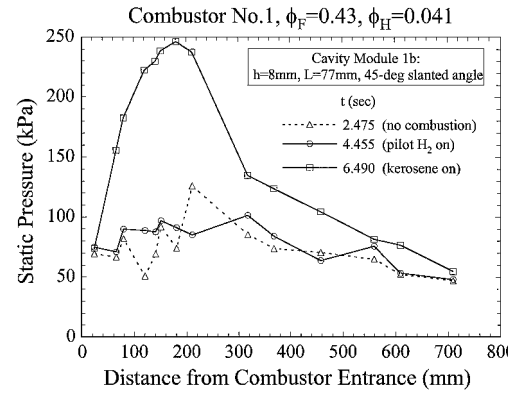


**Fig. 7 Static pressure distributions at relevant moments, using combustor 1 with the integrated cavity module 1b, shown in Fig. 1.**

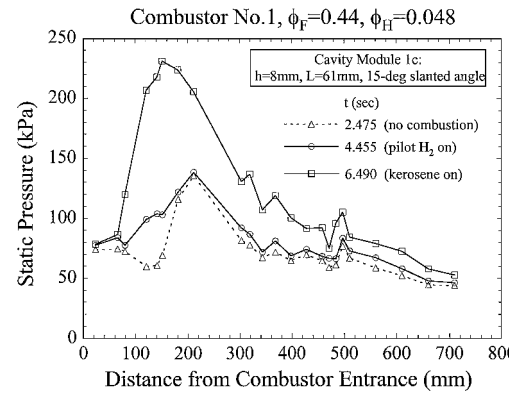


**Fig. 8 Static pressure distributions at relevant moments, using combustor 1 with the integrated cavity module 1c, shown in Fig. 1.**

conditions were kept approximately identical, as listed in Table 1. In addition, Fig. 11 shows the measured profiles of static pressure obtained by injecting the kerosene at the location upstream of the pilot hydrogen station, namely, using the integrated module 1f (Fig. 1). Table 1 also lists the corresponding experimental conditions related to Fig. 11.

We first note that regardless of the differences in the cavity geometry and the injection location of kerosene (either upstream or downstream of the pilot hydrogen station), it is seen from Figs. 6–11 that the position of the peak pressure is similar (although located farther downstream for module 1d). However, the magnitude of the static pressure rise varied from 2.5 to 3.4 times the combustor entrance pressure. Moreover, the corresponding $\phi_{H,min}$ required to sustain kerosene combustion can differ remarkably for various cavity geometries. For example, the highest value of $\phi_{H,min}$ among the six cases was 0.086 for the configuration with the integrated

**Table 1 Experimental parameters and combustion performance of combustor 1[a]**

| Cavity module | Cavity length, mm | Aft ramp angle, deg | Stagnation temperature $T_t$, K | Stagnation pressure $P_t$, MPa | Pilot $H_2$ equivalence ratio $\phi_H$ | Kerosene equivalence ratio $\phi_F$ | Combustion efficiency, % | Total pressure recovery, % |
|---|---|---|---|---|---|---|---|---|
| 1a | 45 | 45 | 1720 | 1.35 | 0.086 | 0.43 | 54 | 44 |
| 1b | 77 | 45 | 1710 | 1.35 | 0.041 | 0.43 | 56 | 45 |
| 1c | 61 | 15 | 1730 | 1.3 | 0.048 | 0.44 | 54 | 44 |
| 1d | 61 | 45 | 1710 | 1.41 | 0.045 | 0.47 | 56 | 43 |
| 1e | 61 | 90 | 1720 | 1.35 | 0.027 | 0.48 | 55 | 43 |
| 1f | 61 | 45 | 1620 | 1.27 | 0.026 | 0.51 | 55 | 42 |

[a]Cavity depth $h = 8$ mm.

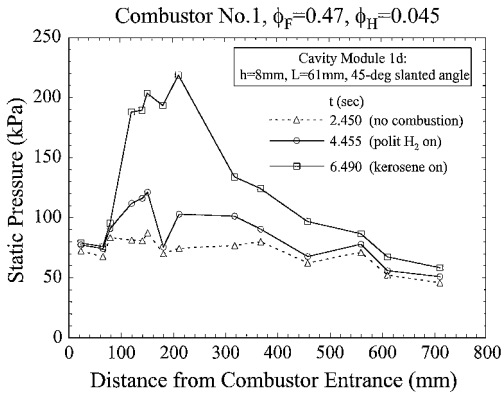


**Fig. 9 Static pressure distributions at relevant moments, using combustor 1 with the integrated cavity module 1d, shown in Fig. 1.**

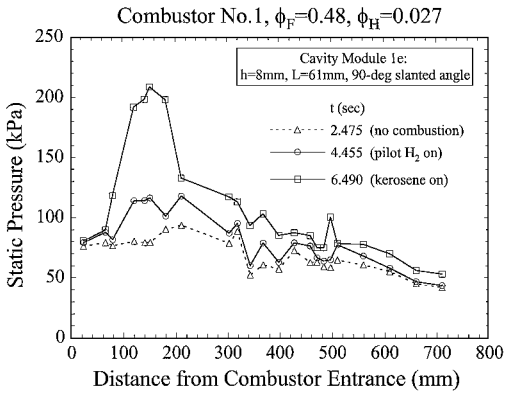


**Fig. 10 Static pressure distributions at relevant moments, using combustor 1 with the integrated cavity module 1e, shown in Fig. 1.**

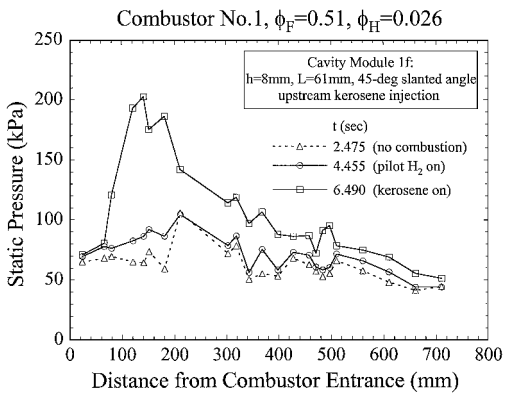


**Fig. 11 Static pressure distributions at relevant moments, using combustor 1 with the integrated cavity module 1f, shown in Fig. 1.**

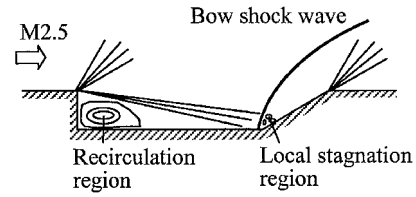


**Fig. 12 Schematic of wave systems in a recessed cavity.**

module 1a, in which $h = 8$ mm and $L = 45$ mm. Because of this larger hydrogen addition, unlike the other five cases, Fig. 6 shows that the static pressure profile when only the pilot hydrogen was injected, that is, $t = 4.455$ s, was different from the baseline pressure profile, that is, $t = 2.475$ s. In addition, it was found that, for the cavity modules 1b–1f, $\phi_{H,min}$ was reduced to 0.026–0.048 when $L/h > 7$, with various slanted angles and regardless of if kerosene was injected either upstream or downstream of the pilot hydrogen station. These results further substantiate our previous finding[19] that the ratio of $L/h$ is the major factor affecting the minimally required pilot hydrogen, whereas the slanted angle of the aft wall and the injection location of kerosene are relatively less important.

Furthermore, the present results seem to suggest that the cavity length of $L/h = 7$–10 would be an optimal configuration, below which more pilot hydrogen is required. If the distance between the injection stations of kerosene and pilot hydrogen or the cavity length were not long enough, the pilot hydrogen flame could not fully develop to produce a sufficient pool of heat and radicals for effecting kerosene ignition. Moreover, if the pilot hydrogen flame was not fully developed, the cold kerosene spray could even quench it. As a result, an increasing amount of pilot hydrogen would be required for the cases of smaller $L/h$.

According to the definition in Refs. 14 and 15, a cavity with length to depth ratio of $5 \sim 9$ might be considered as an open cavity, whereas the cavity with $L/h$ ratio of 10 was referred to as closed. Baurle and Gruber[15] also pointed out that a self-sustaining pressure oscillation could be established in an open cavity. On the other hand, for a closed cavity the shear layer impinges somewhere on the cavity floor rather than the aft wall.[15] Note that the length of the cavity typically determines the characteristics of mass entrainment, whereas the cavity depth essentially characterizes the cavity residence time. However, we have to recognize that these considerations on the open and closed cavities were mainly based on the nonreacting flows. Therefore, it is reasonable to expect that the threshold value of $L/h$ defining the open or closed nature of a cavity may require revisions for complex reacting flows. For instance, the flow-induced resonance might be interfered with and suppressed by the fuel injection into the cavity.[29] In addition, the injection and the subsequent combustion of pilot hydrogen and kerosene inside the cavity can significantly alter the overall flow pattern. We will demonstrate in the following discussion that the threshold value of $L/h$ ratio can be quite different for nonreacting and reacting flows.

We note that all of the cavity modules investigated herein should be considered as open cavities according to the $L/h$ definition of Refs. 14 and 15. However, the present experimental results showed that all of the cavities in fact exhibited a closed nature even with $L/h = 5$–7. Especially, the present closed characteristics can be shown (see Fig. 12). Although according to the present experimental

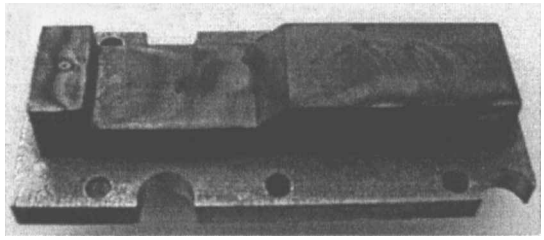

*L/h* = 5.625

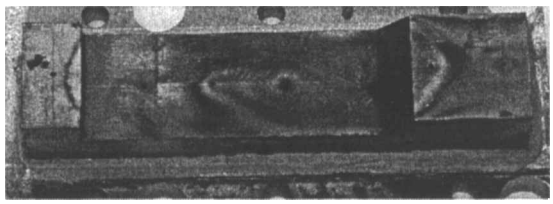

*L/h* = 7.625

**Fig. 13 Direct photographs of two different integrated cavity modules after experiments.**

findings there indeed existed a high-temperature region in the cavity to produce a hot pool for sustaining kerosene combustion, this hot pool was more likely caused by the closed cavity characteristics in which a bow shock wave stands at the rear end of the cavity. Thus, the flow tended to stagnate behind the bow shock and, hence, formed a local high-temperature region therein, as shown in Fig. 12.

Figure 12 was further substantiated by examining the surface color of the two cavity modules, $L/h = 5.625$ (module 1a) and 7.625 (module 1d), after a series of experiments. A direct image shown in Fig. 13 revealed that the temperature distribution in the cavity was extremely nonuniform. In particular, the temperature in the recirculation zone was expected to be relatively low because the local surface color was almost unchanged before and after the experiments. However, there was severe change in the surface color in the local stagnation region near the aft slanted wall, thereby implying a localized high temperature therein. Because there existed a local high temperature, it is reasonable to expect that this local high-temperature region, which possibly acted as a hot pool, would be the major factor in promoting the initiation and the subsequent flameholding of kerosene combustion. Nevertheless, the present results suggest that the threshold value of the length-to-depth-ratio defining a closed cavity should be no more than 5–7 for reacting flows along with mass injection out of the cavity, which is, however, much smaller than the threshold value found in nonreaction flows.

### Influence of Combustor Scaling on $\phi_{H,min}$

Further experiments were carried out using combustor 2. Note that combustor 2 had a larger cross section and longer sections than combustor 1. However, it was found that the cavities, which worked well in combustor 1, were no longer functioning in combustor 2. Therefore, a scaling effect evidently exists. This scaling effect was investigated by 1) increasing the cavity depth from 8 to 12 mm and 2) using two cavities in tandem. For the latter case, one cavity module was installed in the constant area section (section I) and the other identical one was install in the first divergent section (section II) of the combustor.

Figures 14–16 show the measured static pressure distributions yielded by using cavities 2a ($h = 8$ mm and $L = 61$ mm), 2b ($h = 12$ mm and $L = 61$ mm), and 2c ($h = 12$ mm and $L = 95$ mm) (Fig. 2). Figure 17 shows the static pressure distribution when two cavities in tandem are used, where the cavity geometry is the same as cavity module 2c. Detailed experimental information is listed in Table 2.

A comparison of cavity modules 2a and 2b (both are of similar cavity length) results under the same experimental conditions demonstrated that the overall pressures within the constant area section (section I) were much higher in module 2b than those in module 2a, even though $\phi_H$ was about the same for both cases. This in turn suggests that the 8-mm depth might be too shallow to

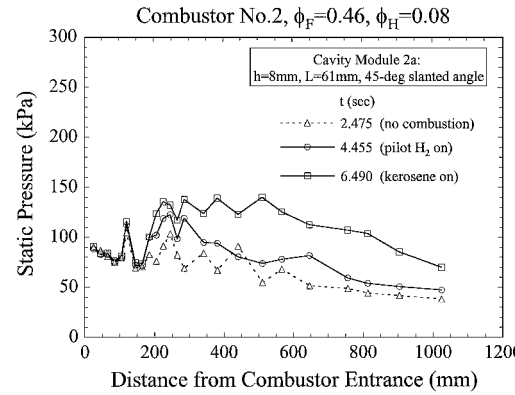


**Fig. 14 Static pressure distributions at relevant moments, using combustor 2 with the integrated cavity module 2a, shown in Fig. 2.**

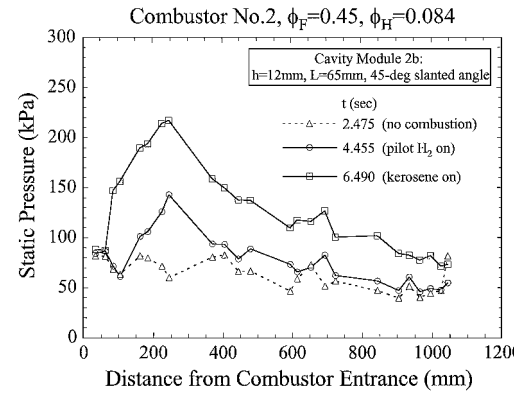


**Fig. 15 Static pressure distributions at relevant moments, using combustor 2 with the integrated cavity module 2b, shown in Fig. 2.**

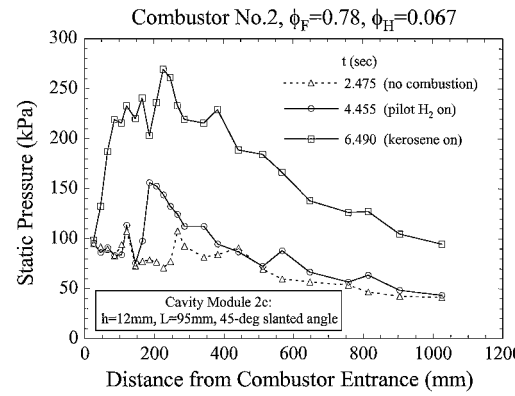


**Fig. 16 Static pressure distributions at relevant moments, using combustor 2 with the integrated cavity module 2c, shown in Fig. 2.**

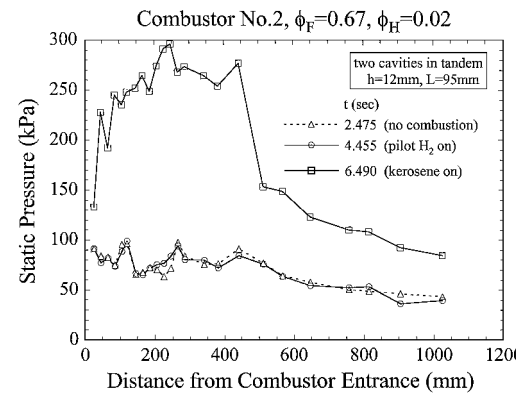


**Fig. 17 Static pressure distributions at relevant moments, using combustor 2 with two cavities in tandem.**

**Table 2 Experimental parameters and combustion performance of combustor 2[a]**

| Cavity module | Cavity depth, mm | Cavity length, mm | Stagnation temperature $T_t$, K | Stagnation pressure $P_t$, MPa | Pilot $H_2$ equivalence ratio $\phi_H$ | Kerosene equivalence ratio $\phi_F$ | Combustion efficiency, % | Total pressure recovery, % |
|---|---|---|---|---|---|---|---|---|
| 2a | 8 | 61 | 1836 | 1.14 | 0.08 | 0.46 | —— | —— |
| 2b | 12 | 61 | 1751 | 1.26 | 0.084 | 0.45 | —— | —— |
| 2c | 12 | 95 | 1811 | 1.17 | 0.067 | 0.78 | 86 | 32 |
| Two cavities in tandem | 12 | 95 | 1691 | 1.11 | 0.02 | 0.67 | 83 | 35 |
| Two cavities in tandem | 12 | 95 | 1637 | 1.13 | 0.037 | 0.65 | 83 | 36 |

[a]Aft ramp angle is 45 deg.

yield sufficient residence time for the complete combustion of the kerosene–air mixture in the recirculation zone. As a result, only a small amount of combustion energy was released immediately after the injection of kerosene in the constant area section. Therefore, the effect of the cavity depth on both ignition and combustion characteristics of kerosene is rather evident.

In addition, for the same cavity depth ($h = 12$ mm), Figs. 15 and 16 compare the combustion characteristics of kerosene with the change in the cavity length from 65 mm (module 2b) to 95 mm (module 2c). Based on the comparison of the static pressure profiles, it appeared that the case using module 2c yielded higher combustion efficiency than that using module 2b. However, note that the required pilot hydrogen equivalence ratio still remained high, for instance $\phi_{H,min} \sim 0.067$, even when module 2c was used. In addition, because of the relatively high hydrogen equivalence ratio, the pressure rise due to the pilot hydrogen combustion was noticeable, as shown in Fig. 16 for the static pressure profile at $t = 4.455$ s.

Figure 17 shows the pressure distributions at various instants for the case with two cavities in tandem, when $\phi_H = \phi_{H,min}$. Because of the collective actions of two cavities in tandem, the minimally required pilot hydrogen equivalence ratio can be as low as 0.02. It is also rather evident that the difference in the static pressure profile was very little before and after the pilot hydrogen injection. This result further indicates that the flameholder mechanism with two cavities in tandem seems to be more effective than that using a single cavity module. However, the controlling mechanism leading to better performance in the case with two cavities in tandem is not yet fully understood. One possible mechanism is due to the cavity resonance, which can result in periodic shedding of organized structures that can in turn be used to control flowfields. Nonetheless, the two high-temperature regions in the configuration with two cavities in tandem, each would behave in the similar manner as shown in Fig. 12, must play an important role in reducing ignition delay time and sustaining a stable kerosene combustion.

These results clearly demonstrate that, although ignition characteristics were indeed improved with increasing cavity depth, more significant improvement was made by two cavities in tandem. Moreover, although the scaling effect indeed existed, the minimally required pilot hydrogen equivalence ratio as low as 0.02 for the ignition enhancement, and combustion stabilization of kerosene was achievable.

### Combustion Efficiency and Total Pressure Recovery

To assess the combustor performance, a one-dimensional model[20,21] has been developed. In particular, the flowfield within the combustor has to be approximated based on the experimental static pressure data. Thus, the measured profile of static pressure was first fitted and was subsequently used as an input to compute axial profiles of Mach number, static pressure, total pressure, static temperature, total temperature, and core flow area. Figures 18 and 19, respectively, show the typical flowfields corresponding to combustors 1 and 2, in which all data except Mach number are in units of the corresponding combustor entrance condition. The experimentally measured static pressure data are also plotted as a reference. In general, the approximate flowfield is reasonable and consistent with the experimental observation and, hence, the one-dimensional model

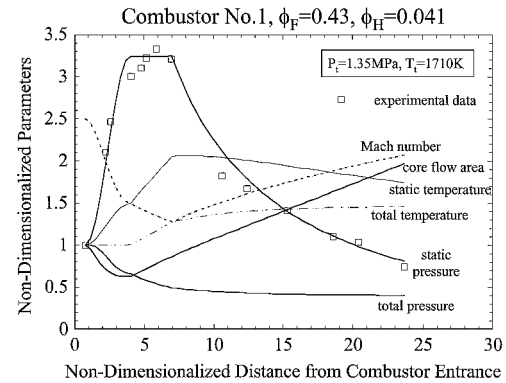


**Fig. 18 Typical characterization of the flowfield within combustor 1.**

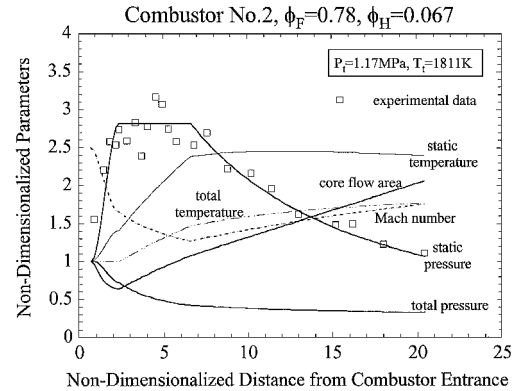


**Fig. 19 Typical characterization of the flowfield within combustor 2.**

greatly facilitates data analyses. We nevertheless have to point out that the actual flowfield is full of shocks, expansion waves, boundary separation, and their mutual interactions. Those complications, however, were not considered in this simplified model.

Figure 18 also shows that for combustor 1 the static temperature first increased rapidly to a peak value and then continuously decreased till the combustor exit. On the contrary, the static temperature in combustor 2 increased to a steady value, as shown in Fig. 19. Such a different response in the static temperature distribution can be attributed to the difference in the effective equivalence ratio of kerosene. Especially, combustor 2 had a larger $\phi_F$ so that the heat release was expected to more substantial. Note that the combustion efficiency is generally defined by the ratio of the static temperature increment between the exit and entrance of combustor to the temperature difference between the corresponding adiabatic flame temperature and the static temperature at entrance. Thus, the static temperature at the combustor exit has a significant effect on the overall combustion efficiency.

Table 1 lists typical combustor performance of combustor 1 using various integrated cavity modules. For the conditions tested, the stagnation temperature and stagnation pressure were mostly kept around 1700 K and 1.35 MPa, respectively, while the kerosene equivalence ratios were around 0.5. It was found that the minimally

required pilot hydrogen equivalence ratios varied from 0.086 to 0.026. However, the combustion efficiency for all six cavity modules was about the same, ~55%. This in turns suggests that the cavity configuration might not have significant effect on the combustion efficiency, although it does affect the minimally required pilot hydrogen equivalence ratio. Moreover, the total pressure recoveries for the six modules were all around 45%.

Table 2 lists typical performance of combustor 2 using various integrated cavity modules. The stagnation temperature ranged from 1630 to 1830 K, and the stagnation pressure was kept around 1.13 MPa. The kerosene equivalence ratio varied from 0.45 to 0.78, and the minimally required pilot hydrogen equivalence ratio varied from 0.084 to 0.02. Furthermore, Table 2 shows that the combustion efficiency of kerosene combustion in a well-designed combustor can be more than 80%, whereas the corresponding total pressure recovery was seen to drop below 40%.

## Summary

Investigations on the ignition and combustion characteristics of kerosene were conducted using two model combustors of cross sections 30.5 × 30 mm and 51 × 70 mm, respectively. The entry Mach number was fixed at 2.5. Various types of pilot and flameholder integrated modules were tested. The total pressure of vitiated air varied from 1.1 to 1.8 MPa and the total temperature ranged from 1500 to 1900 K.

It was estimated that for the temperature range of 1000–1500 K, the evaporation time of kerosene droplet could be limited to within 1 ms if the droplet diameter is smaller than 20 $\mu$m. In addition, the mean diameter of the kerosene spray generated was measured to be around 20–25 $\mu$m with injection pressure varied from 2.5 to 4.5 MPa. Furthermore, visualization of kerosene atomization revealed that the penetration and spreading of kerosene jet spray increased by 30% with increasing injection pressure from 2.5 to 4.5 MPa.

Results demonstrated that the parallel pilot hydrogen injection was not the most effective scheme to promote the ignition and flameholding of kerosene, as compared to the normal injection scheme as well as the combined parallel–normal injection scheme. Therefore, the adequate distribution of pilot hydrogen inside the cavity was shown to be critical.

It was also found that the temperature distribution in the cavity was extremely nonuniform. Because there existed rather high temperature locally, it is reasonable to expect that this local high-temperature region somewhere in cavity may act as a hot pool of heat and radicals, which in turn is the major factor to promote ignition and flameholding.

The scheme with two cavities in tandem was further shown to be a more effective flameholder mechanism than that with a single cavity. For the configuration with two cavities in tandem, there existed complex cavity resonance and high-temperature region associated with each cavity module. These collective effects play an important role in reducing ignition delay time and sustaining stable combustion of kerosene. Further study in this regard is warranted.

Although the scaling effect was shown to exist, the minimally required pilot hydrogen equivalence ratio can be as low as 0.02 in the present kerosene-fueled combustor. Furthermore, based on a simplified one-dimensional model, the combustion efficiency of kerosene in well-designed combustors can be more than 80%, while the corresponding total pressure recovery was around 35%.

Finally, for the success of applying the recessed cavity flameholders in liquid hydrocarbon-fueled scramjet propulsion systems, it is imperative that the cavity residence time is sufficiently long to sustain the hot pool of combustion products. Therefore, this residence time (at least) has to be larger than the sum of the liquid fuel vaporization time and the ignition delay time. Following the definition of Ref. 15, the cavity residence times of the integrated cavity modules employed herein were estimated to range from 1.8 to 3 ms. As such, for the present kerosene–hydrogen system it is crucial that the mean droplet size of the kerosene spray is smaller than 20 $\mu$m and the local high temperature is higher than 1280 K to meet the leading-order criterion.

## Acknowledgments

Current research program was supported by the National Natural Science Foundation of the People's Republic of China through Contract 19789202. C. J. Sung was supported by the Case School of Engineering through the Case Alumni Association. The authors would also like to acknowledge D. X. Qian and Y. Li for their assistance in experimental preparations, and S. L. Xu, L. J. Ji, and B. K. Zheng for help with data reduction.

## References

[1]Tishkoff, J. M., Drummond, J. P., Edwards, T., and Nejad, A. S., "Future Direction of Supersonic Combustion Research: Air Force/NASA Workshop on Supersonic Combustion," AIAA Paper 97-1017, Jan. 1997.

[2]Waltrup, P. J., "Liquid Fueled Supersonic Combustion Ramjets: A Research Prospective of the Past, Present and Future," *Journal of Propulsion and Power*, Vol. 8, No. 6, 1987, pp. 515–524; also AIAA Paper 86-0158, Jan. 1986.

[3]Bonghi, L., Dunlap, M. J., Owens, M. G., Young, C., and Segal, C., "Hydrogen Piloted Energy for Supersonic Combustion of Liquid Fuels," AIAA Paper 95-0730, Jan. 1995.

[4]Avrashkov, V., Baranovsky, S., and Levin, V., "Gasdynamic Features of Supersonic Kerosene Combustion in a Model Combustor Chamber," AIAA Paper 90-5268, Oct. 1990.

[5]Kay, I. W., Peschke, W. T., and Guile, R. N., "Hydrocarbon-Fueled Scramjet Combustor Investigation," *Journal of Propulsion and Power*, Vol. 8, No. 2, 1992, pp. 507–512.

[6]Vinogradov, V., Kobigsky, S., and Petrov, M., "Experimental Investigation of Liquid Hydrocarbon–Hydrogen Fuel Combustion in Channel at Supersonic Velocities," AIAA Paper 92-3429, July 1992.

[7]Morrison, C. Q., Campbell, R. L., Edelman, R. B., and Jaul, W. K., "Hydrocarbon Fueled Dual-Model Ramjet/Scramjet Concept Evaluation," *Proceedings of the International Symposium on Air Breathing Engines*, ISABE Paper 97-7053, Sept. 1997.

[8]Ju, Y., and Nioka, T., "Ignition Simulation of Methane/Hydrogen Mixtures in a Supersonic Mixing Layer," *Combustion and Flame*, Vol. 102, No. 4, 1995, pp. 462–470.

[9]Ortwerth, P., Mathur, A., Vinigragov, V., Grin, V., Goldfeld, M., and Starov, A., "Experimental and Numerical Investigation of Hydrogen and Ethylene Combustion in a Mach 3–5 Channel With a Single Injector," AIAA Paper 96-3245, July 1996.

[10]Owens, M., Segal, C., and Auslender, A. H., "Effects of Mixing Schemes on Kerosene Combustion in a Supersonic Airstream," *Journal of Propulsion and Power*, Vol. 13, No. 4, 1997, pp. 525–531.

[11]Lanovski, L. S., and Moses, C., "Endothermic Fuels for Hypersonic Aviation," AGARD Meeting on Fuels and Combustion Technology for Advanced Aircraft Engines, May 1993.

[12]Jackson, K., Corporan, E., Buckley, P., Leingang, J., Karpuk, M., Dippo, J., Hitch, B., Wickham, D., and Yee, T., "Test Results of an Endothermic Fuel Reactor," AIAA Paper 95-6028, April 1995.

[13]Segal, C., Owens, M. G., Tehranian, S., and Vinogradov, V., "Flameholding Configurations for Kerosene Combustion in a Mach 1.8 Airflow," AIAA Paper 97-2888, July 1997.

[14]Yu, K., Wilson, K. J., Smith, R. A., and Schadow, K. C., "Experimental Investigation on Dual-Purpose Cavity in Supersonic Reacting Flows," AIAA Paper 98-0723, Jan. 1998.

[15]Baurle, R. A., and Gruber, M. R., "A Study of Recessed Cavity Flowfields for Supersonic Combustion Applications," AIAA Paper 98-0938, Jan. 1998.

[16]Owens, M., and Segal, C., "Combustion of Kerosene in a Supersonic Airstream—Thermal Efficiency of Selected Injection Configurations," AIAA Paper 96-3140, July 1996.

[17]Baurle, R. A., Mathur, T., Gruber, M. R., and Jackson, K. R., "A Numerical and Experimental Investigation of a Scramjet Combustion for Hypersonic Missile Applications," AIAA Paper 98-3121, July 1998.

[18]Ben-Yakar, A., and Hanson, R. K., "Cavity Flameholders for Ignition and Flame Stabilization in Scramjets: Review and Experimental Study," AIAA Paper 98-3122, July 1998.

[19]Li, J. G., Yu, G., Zhang, X. Y., and Huang, Q. S., "Combustion of Kerosene in a Supersonic Stream," AIAA Paper 2000-0615, Jan. 2000.

[20]Yu, G., Li, J. G., Zhao, J. R., Qian, D. X., Han, B., and Li, Y., "Hydrogen–Air Supersonic Combustion Study by Strut Injectors," AIAA Paper 98-3275, July 1998.

[21]Yu, G., Li, J. G., Zhao, J. R., Han, B., Chang, X. Y., and Qian, D. X., "Experimental Studies on $H_2$/Air Model Scramjet Combustor," AIAA Paper 99-2449, June 1999.

[22]Li, J. G., Yu, G., Zhang, Y., Li, Y., and Qian, D. X., "Experimental Studies on Self-Ignition of Hydrogen/Air Supersonic Combustion," *Journal of Propulsion and Power*, Vol. 13, No. 4, 1997, pp. 538–542.

[23]Kanury, A. M., *Introduction to Combustion Phenomena*, Gordon and Breach, New York, 1977, pp. 142–179.

[24]Veretennicov, V. G., "Autoignition Study on Kerosene in Supersonic Flow," Moscow Aviation Inst., Rept. SPC 96-4089, Moscow, Russia, Oct. 1997.

[25]Mullins, B. P., "Studies on the Spontaneous Ignition of Fuels Injected into a Hot Air-Stream Part II: Effect of Physical Factors upon the Ignition Delay of Kerosene-Air Mixtures," *Fuel*, Vol. 32, 1953, pp. 234–252.

[26]Wang, T.-S., "Thermo-Kinetics Characterization of Kerosene/RP-1 Combustion," AIAA Paper 96-2887, July 1996.

[27]Sung, C. J., Li, J. G., Yu, G., and Law, C. K., "Chemical Kinetics and Self-Ignition in a Model Supersonic Hydrogen-Air Combustor," *AIAA Journal*, Vol. 37, No. 2, 1999, pp. 208–214; also AIAA Paper 98-0722, Jan. 1998.

[28]Yu, G., Law, C. K., and Wu, C. K., "Laminar Flame Speed of Hydrocarbon + Air Mixtures with Hydrogen Addition," *Combustion and Flame*, Vol. 63, 1986, pp. 339–347.

[29]Burnes, R., Parr, T. P., Wilson, K. J., and Yu, K., "Investigation of Supersonic Mixing Control Using Cavities: Effect of Fuel Injection Location," AIAA Paper 2000-3618, July 2000.